frontiers | Frontiers in Physics

TYPE Original Research
PUBLISHED 02 March 2023
DOI 10.3389/fphy.2023.1160287

OPEN ACCESS

EDITED BY
Shuo Liu,
Hebei University of Technology, China

REVIEWED BY
Hailiang Chen,
Yanshan University, China
Wei Liu,
Zhejiang Agriculture and Forestry University, China
Chen Shi,
National University of Defense Technology, China

*CORRESPONDENCE
Yingbin Xing,
jsxyb1232008@126.com

SPECIALTY SECTION
This article was submitted to Optics and Photonics, a section of the journal Frontiers in Physics

RECEIVED 07 February 2023
ACCEPTED 20 February 2023
PUBLISHED 02 March 2023

CITATION
Cai Y, Mai Y, Xiang S, Shi J, Zhu Q, Li R, Li J, Li C, Yan D and Xing Y (2023), Flexible beam delivery of ultrafast laser through vacuum-pumped anti-resonant hollow-core fiber.
Front. Phys. 11:1160287.
doi: 10.3389/fphy.2023.1160287

Flexible beam delivery of ultrafast laser through vacuum-pumped anti-resonant hollow-core fiber

Yiming Cai[1], Yifan Mai[2], Shen Xiang[1], Jianhong Shi[1], Qixin Zhu[1], Rong Li[2], Jinyan Li[1], Cheng Li[1], Dapeng Yan[1] and Yingbin Xing[1]*

[1]Huazhong University of Science and Technology, Wuhan, China, [2]Wuhan Raycus Fiber Laser Technologies Co., Ltd., Wuhan, China

We demonstrate the transmission of a 100 MW-peak-power ultrafast laser through a 5-m anti-resonant hollow-core fiber (AR-HCF) with a pumpable armored tube for air exhaust. The AR-HCF consists of a 45-μm-hollow-core and seven untouched capillaries with an attenuation of 0.11 dB/m measured at a wavelength of 1030 nm. We investigate the effect of air-filling and vacuum pumping on transmission efficiency and pulse distortion. The comparison reveals the importance of controlling air concentration in hollow-core fibers (HCFs) for achieving high transmission efficiency and pulse quality. With the suppression of air concentration, the transmission efficiency increases from 61% to 72%, and pulse distortion is effectively controlled. The results demonstrate the potential of AR-HCFs for high-power ultrafast laser delivery systems for various applications. The pumpable armored tube design provides a simple and effective solution to suppress self-phase modulation (SPM) and enable flexible beam delivery.

KEYWORDS

anti-resonant fiber, AR-HCF, flexible beam delivery, vacuum-pumped HCF, ultrafast laser delivery

1 Introduction

Ultra-fast laser sources with picosecond or femtosecond laser pulses have shown a wide range of application in micro-and nanofabrication [1–4]. The peak power intensity of ultrafast lasers determines the characteristics of their free-space transport structure, which to some extent increases the possible instability of the laser over a long period of time [5]. In contrast to fiber-delivered nanosecond or continuous lasers, ultrafast lasers are difficult to propagate in traditional silica fibers because the non-linear effects during fiber delivery and the pulse peak fluence induced self-focusing might exceed the damage threshold of those fibers [6]. Since 1999, researchers have examined the viability of employing a HCF to transmit laser beams in an effort to address the issue of flexible delivery of short-pulse laser beams [7]. Compared to the photonic-bandgap hollow-core fibers (PB-HCFs) [8], the AR-HCFs feature a comparatively simple micro-structured cladding [9] and a broad transmission bandwidth [10], which makes them suited for wide-spectrum, high peak power beam transmission. It has been reported that the visible spectral range lasers, which are generated by the use of second-harmonic generation (SHG) and third-harmonic generation (THG) of fiber or Nd: YAG ultrafast laser sources, have shown the achievement in beam flexible transmission of green [11] and ultraviolet [12, 13] lasers. The AR-HCF with cladding-tubes-touched structure has been utilized to transmit lasers with

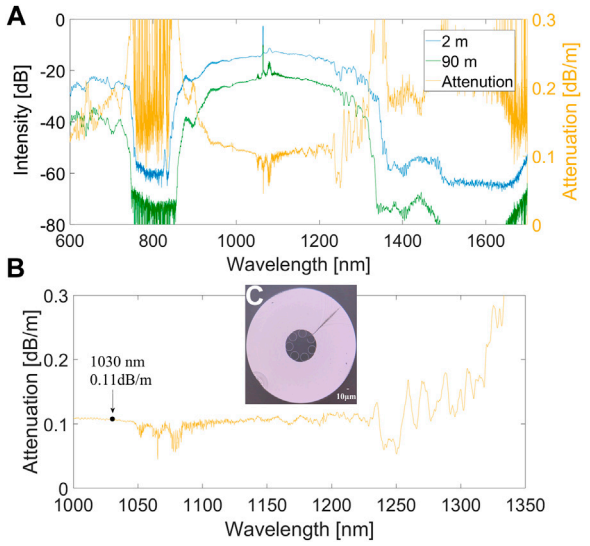

FIGURE 1
(A) Measured transmission spectra of the 2 m (solid blue curve) and the 90 m (solid green curve) AR-HCF and attenuation spectrum (solid yellow curve) in the range of 600 nm–1700 nm. **(B)** Detailed attenuation spectrum measured in the near-infrared range of 1,000 nm–1,350 nm (solid yellow curve). **(C)** Cross setion of seven capillaries AR-HCF with 45-μm-core diameter.

transmission bands ranging from 1 μm to 4 μm [14–16]. The 0.11 dB/m transmission losses of an ice-cream-structure AR-HCF have enabled the demonstration of a laser with a 63.1% coupling efficiency at 1,064 nm [17]. Theoretical advancements have indicated that AR-HCF fibers without nodes are being studied to reduce transmission loss [18, 19]. Recent studies have demonstrated a node-less AR-HCF for a 300 W laser guidance at 1,080 nm with a 0.05 dB/m attenuation [20]. Studies have shown a much higher transmission power of 1.167 kW with a high efficiency of 87.5% at the adjacent wavelength of 1,070 nm, by using an ice-cream structure AR-HCF [21]. Although HCFs have lower non-linear effects [22] and higher power damage thresholds [23] compared to conventional silica solid fibers, the effect of non-linearity could not be ignored for the laser transmission process of ultrafast lasers with high peak power over 30 MW [24]. Ultra-fast laser pulses transmitted along the HCFs have enough energy to interact with the air or gas in the hollow core to introduce the pulse chirp and thus broadening the pulse duration [25–27]. Factors found to be influencing power transmission limitations have been explored in several studies that show non-linear effects such as Raman scatting and SPM have played a critical role in ultra-fast laser delivering efficiency [28, 29]. Filling inert gas or vacuum states has been demonstrated and mentioned in research analyses as an effective method to modulate the non-linear effects in the beam transmission process [29–31]. Published studies have used gas-filled HCFs for spectral broadening and chirped mirror systems to compensate for dispersion and to compress for a shorter pulse duration [32–34]. However, the pulse recompression process lets the flexible beam delivery transfer to spatial transmission. Although there are proposed theoretical models showing that light transmission in the photonic crystal fibers of a negative refractive index metamaterial could compensate for dispersion [35]; however, this has not been achieved in practice. Our objective is to accomplish ultrafast laser transmission while keeping the light source's original properties. In this research, a vacuum chamber is concerned with preventing gas interactions and decreasing non-linear effects. The flexible beam delivery utilizes a 5-m AR-HCF with an attenuation of 0.11 dB/m at 1,030 nm. Laser transmission in air-filled and vacuum-pumped fiber is discussed separately. The pulsed laser is transmitted through an air-filled HCF, and the SPM interferes with the dispersion balance of the ultra-fast laser system, with a pulse spread of 16.5 ps. With the suppression of air concentration, the power transmission efficiency improves from 61% to 72% and the pulse duration is observed with slightly broadening from 500 fs to 670 fs.

2 Fiber structure and experimental setup

2.1 Fiber characteristic

The cross section of the fabricated AR-HCF fiber is shown in Figure 1C, which consists of seven untouched capillaries with an inscribed core diameter of 45 μm and a mode field diameter of 35 μm, the outer diameter of the capillaries of 22.6 μm and the jacked diameter of 314 μm. For multi-capillary anti-resonant fibers, the suppression of higher order modes (HOMs) is achieved with the increasing number of cladding holes, which is confirmed in Refs. [19, 36]. Moreover, bending loss of the AR-HCF could be suppressed by designing a smaller-core size [37]. The wall thickness of the capillaries and the gap distance between the capillaries also affect the transmission loss [19]. However, the increasing number of cladding capillaries and small core size are accompanied by a reduction in the fundamental mode field area, necessitating careful laser coupling to the AR-HCF [38]. The fundamental mode loss, bending loss and coupling efficiency are comprehensively considered for the future application, and the AR-HCF with mentioned parameters are designed and fabricated. The theoretical fundamental mode attenuation is calculated to be 0.89 dB/km at 1,030 nm by the expression discussed in Ref. [39].

The transmission spectra of the AR-HCF is measured by using a broadband light source (NKT Photonics) and a YOKOGAWA spectrometer, as shown in Figure 1A. The attenuation curve of wavelength from 600 nm to 1700 nm, as measured by the cut-back method (cut the 90 m fiber to 2 m). Figure 1B depicts the detailed decay curves covering the laser range from 1,000 nm to 1,350 nm. The positioning and deformation of the capillaries during fiber drawing, as well as the beam quality of the laser source, might result in variations between the theoretical and measured values. The calculated mode loss of LP01, LP11, and LP21 are 0.89 dB/km, 3.17 dB/km and 1.24 dB/km, respectively.

The low transmission loss is the combined result of the control of capillary and inter-capillary spacing consistency during the fiber drawing process as shown in Figure 1C. Measured transmit loss is 0.11 dB/m at 1,030 nm, which is much higher than the theoretical value, despite this, it shows an improvement comparison with a similar-structure seven capillaries AR- HCF in the most recent published article [40]. It is worth mentioning that the measured

TABLE 1 Performance comparison of recently reported attenuation of seven capillaries AR- HCFs.

Core diameter (μm)	Capillary thickness (μm)	Capillary diameter (μm)	Measured min. loss (dB/m at nm)	Time
28	0.78	18	0.11–1.2 at1,065	2022 [40]
35	0.355	17	0.05 at1,080	2021 [20]
31	0.78	23.6	0.07 at1,064	2021 [41]
28.3	0.43	10.6	0.7 at1,100	2021 [42]
17	0.132	7.3	0.26 at355	2018 [12]
35.8	0.775	7.67	0.028 at1,030	2018 [29]
30	0.83	17	0.03 at1,090	2016 [36]

The bold values are the core diameter of the AR-HCF.

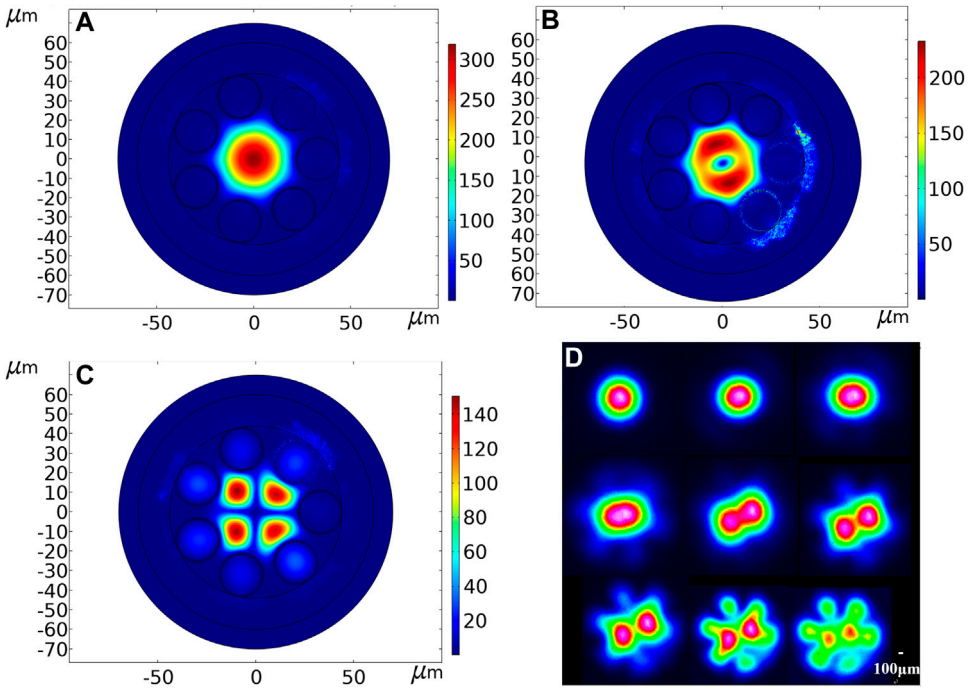

FIGURE 2
(A–C). Simulated mode field distribution of LP01, LP11 and LP31, respectively. **(D)** Measured mode profiles by the misalignment of the incident beam.

transmission loss of HCFs is related to fiber parameters such as core size, capillary diameter, and wall thickness; fiber drawing quality such as roughness; attenuation measurement methods such as fiber length, light source quality, etc. Table 1 summarizes the relevant parameters of seven capillaries AR- HCF published in recent years and their measured attenuation at certain wavelengths for reference.

2.2 Simulated and measured beam profiles

The finite element software COMSOL is used for simulating mode profiles AR-HCF as shown in Figures 2A–C. In the experiment, the focus lens is relocated away from the input side of the AR-HCF to misalign the focus point and stimulate HOMs. Figure 2D depicts the variation of the diameter mode field distribution of LP01 to LP11 obtained by adjusting the focusing mirror shown in Figure 3 to eccentricate the spot, with a fiber coiling diameter of 45 cm. It could be observed from the figure that no HOMs, such as LP21 and LP31, were observed after propagating 5 m. The reason is that the manufactured AR-HCF structure is not homogeneous, resulting in actual attenuation values for HOMs that are greater than their theoretical values. Moreover, the incident beam profile approaches the fundamental mode (M^2 = 1.167), and the contrast of the excited higher-order modes is rather low, so that only the LP01 and LP11 modes with reduced transmit loss could be examined. This result preliminarily shows that transmission in the AR-HCF has the effect of optimizing the beam quality.

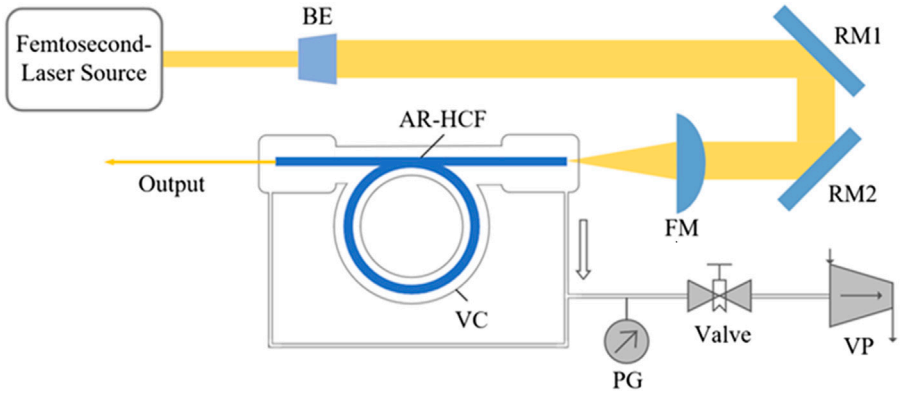

FIGURE 3
Experiment setup of the laser beam transmission system. BE: Beam expander; RM: Reflect mirror; FM: Focus mirror; VC: Vacuum chamber; PG: Pressure gauge; VP: Vacuum pump.

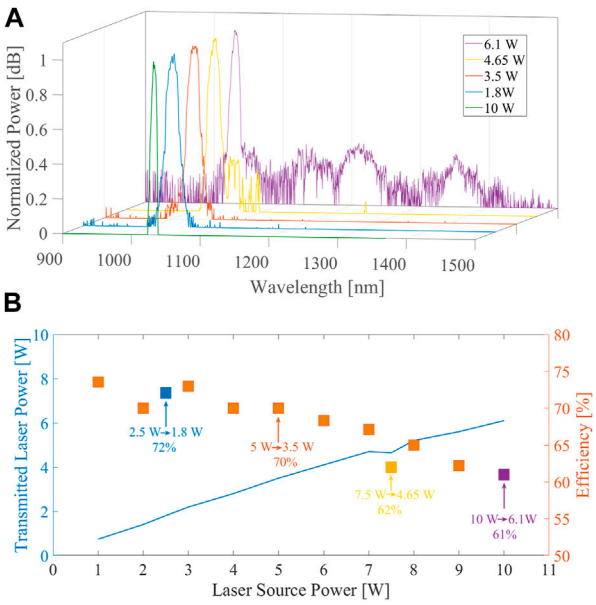

FIGURE 4
(A) Spectrum of the ultra-fast laser source (LS, green curve); Laser transmitted spectra measured after the air-filled AR-HCF: After transmissions, the input laser power drops from 2.5 W to 1.8 W (blue curve), 5 W–3.5 W (orange curve), 7.5 W–4.65 W (yellow curve) and 10 W–6.1 W (purple curve), respectively. **(B)** Transmitted laser power and transmission efficiency versus ultra-fast laser source power.

2.3 Experimental setup

The experimental setup is shown as Figure 3. A self-built 1,030 nm ultra-fast laser source with an average power of 10 W, a pulse duration of 500 fs, and a maximum single pulse energy of 50 μJ is used as the seed laser. The beam quality $M^2 = 1.167$, which is measured by a camera-based beam propagation analyzer (BeamSquared XC130). The output beam diameter is expanded from 1 mm to 2 mm by a beam expander. The two reflectors, RM1 and RM2, are crucial in adjusting the parallelism and perpendicularity of the laser beam. The RM1 and RM2 mirrors have a low group delay dispersion (GDD<30 fs^2) and a coating that ensures reflectance greater than 99.5% from 970 nm to 1,150 nm. The divergence angle of the AR-HCF is 0.035 mrad and the aspherical lens with a collimation distance of 30 mm focuses the beam into the AR-HCF with a focused spot diameter of 23.6 μm. An industrial high-precision optical fiber cleaver (Fujikura CT104 +) is used to cleave AR-HCF, and the cutting angle of the fiber is less than 0.5°. The length of 5 m of AR-HCF is placed inside an evacuable vacuum chamber to reduce gas interactions and minimize non-linear effects. The vacuum chamber is designed as an armored tube that could be coiled with a diameter ranging from 25 cm to 45 cm for flexible beam transmission. The air pressure is regulated by regulating the air flow through the valves, and the barometer is utilized to read the actual air pressure. A spectrum analyzer (YOKOGAWA AQ6370D) is used to record the laser's output spectrum, and an autocorrelator (APE Pulsecheck) is used to measure the pulse duration.

3 Results and discussion

Figure 4A shows the comparison between the measured spectrum of the ultra-fast laser source and the transmitted laser spectra at different laser powers. The spectral range of the femtosecond laser source is over 1,025 nm–1,040 nm, and after propagating through the AR-HCF, the spectral spread covers the range from 1,000 nm to 1,350 nm due to the non-linear effects. The spreading of the laser spectra in AR-HCF and the generation of deformation phenomena of the pulses is a complex non-linear process. Numerous theoretical and practical investigations on the transmission characteristics of ultrafast pulses in AR-HCF have been conducted [29, 30, 39, 43]. However, the mechanism behind their generation is still not fully comprehended. Many non-linear processes, including SPM, stimulated Raman scattering (SRS), four wave mixing, and higher-order soliton splitting, could be

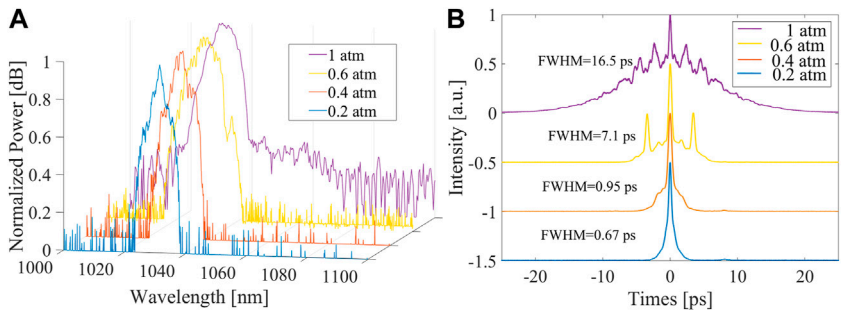

FIGURE 5
(A) Measured 6.1 W-output laser (input laser 10 W) transmission spectra after the vacuum-pumped AR-HCF. The curves from bottom to top show the spectral profiles that obtained under chamber pressure from p = 0.2 atm (blue curve), 0.4 atm (orange curve), 0.6 atm (yellow curve), and 1 atm (purple curve), respectively. **(B)** Autocorrelation curves under different pressures.

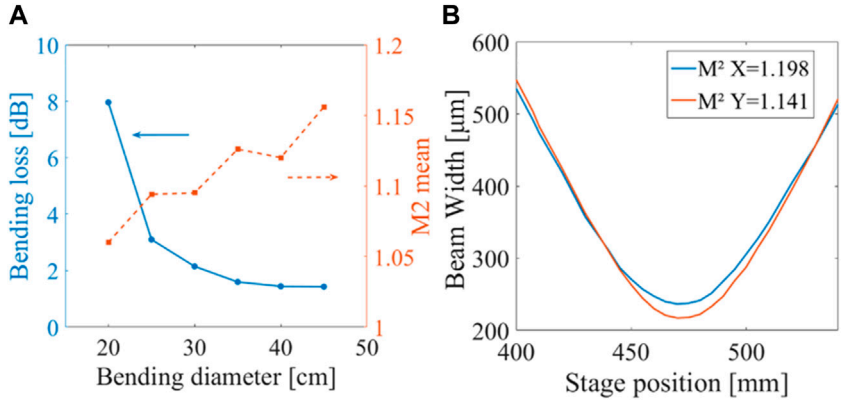

FIGURE 6
(A) Bending loss and M^2 versus bending diameter in the vacuum-pumped AR-HCF. **(B)** Measured laser source beam quality as a function of coiling diameter at 45 cm.

involved in optical pulse transmission [44]. As demonstrated in Figure 4A, the spectrum broadening is mostly caused by the SPM and SRS after laser beam propagation down the air-filled AR-HCF. The SPM phenomena may be detected more clearly if the associated laser power was increased. Since the femtosecond laser source is a broadband source with a measured spectral width of 9.56 nm at full width half maximum, it is going to be difficult to distinguish between the spectral frequency oscillation caused by the SPM and the Raman scattering peaks in the spectral range of 1,020 nm–1,040 nm; nonetheless, the Raman scattering peaks that could be observed in the range of 1,100 nm–1,450 nm at an incident optical power of 10 W. The Raman frequency shift around 1,140 nm, 1,220 nm and 1,350 nm is in agreement with the simulation results in Ref. [29]. The transmitted laser power, and transmission efficiency calculated by the ratio of input power/output power, versus laser source power are shown in Figure 4B. When the peak power of the light source exceeds 50 MW, a significant decrease drops to around 61% in transmission efficiency could be observed. The spectral range of the femtosecond laser source is over 1,025 nm–1,040 nm, and after propagating through the AR-HCF, the spectral spread covers the range from 1,000 nm to 1,350 nm. As the laser power increases, the non-linear effects that cause the spectrum to broaden intensify. This causes laser energy to be shifted to frequencies with higher losses, which leads to a decrease in transmission efficiency.

To reduce the Kerr effect of laser propagation in AR-HCF, we pumped out the air and measure the laser spectra at various air pressures, as shown in Figure 5A. Notably, at a pressure of 0.2 atm, the transmitted laser power increases from 6.1 W to 7.2 W when the input laser power is 10 W. The SPM is alleviated as the air concentration in the chamber decreases. As seen from the autocorrelation results in Figure 5B, the 500-fs laser pulse broadens to 16.5 ps (FWHM, Gaussian fit) after propagating through the 5-m length, air-filled fiber, which indicates that the pulse experiences a large non-linear phase shift in the fiber, enhanced by the SPM, and in agreement with the effect of SPM on pulses discussed in Ref [34]. This indicates that as the air is filled, the pulse waveform is broadened symmetrically, and oscillatory structures appear on both wings of the pulse. This demonstrates that the SPM effect is at work, and that the dispersion-induced non-linear effects are weaker. This is demonstrated by the later analysis:

when the pulse is transmitted in the fiber, both GVD and SPM cause the pulse to produce a frequency chirp, and while the pulse chirp introduced by GVD is linear, the pulse chirp introduced by SPM is far from linear within the whole pulse. Various portions of the pulse transmit at different speeds due to the non-linear character of the post-composite chirp. Especially in the situation of normal dispersion, the redshifted light near the leading edge of the pulse transmits faster than the non-redshifted light at the trailing end of the pulse's front; the opposite is true for the blue shifted light near the following edge. In both instances, the area of the front and rear edges of the pulse contains two different frequencies of light that interfere with one another, and the oscillations around the edge of the pulse are the result of this interference. As the air concentration decreases, the symmetrical oscillation structure of the pulse gradually weakens, which also indicates a gradual decrease of the phenomenon of SPM. The anti-resonant seven-core-touchless capillary hollow fiber is less sensitive to bending loss relative to other mechanisms that have been compared [29].

In our experiment, we investigate the laser propagation bending loss versus fiber coil diameters from 20 cm to 45 cm in the vacuum pumped AR-HCF, as shown in Figure 6A. In this configuration, the coiling diameter is greater than 35 cm, the bending loss is less than 1.5 dB, and the critical coiling value of the fiber is reached when the bending diameter is less than 30 cm. At this point, the fiber bending causes the fiber base mode to higher order mode transition, which causes most of the light to leak from the core, resulting in an increase in power loss. We also determined the relationship between beam quality and bending diameter. Figure 6B shows the measured transmitted laser source beam quality of M^2X = 1.198, M^2Y = 1.141 at the bending diameter of 45 cm. Although the beam quality factors vary only by 0.122 (1.182–1.06) when the fiber coiling diameter is varied in the range of 25 cm–45 cm, the dashed orange curve shows the decrease in the coiling diameter of the fiber is accompanied by a decreasing trend in M^2. The results indicate that the optimal coiling of the AR-HCF fibers could optimize transmission mode distribution.

4 Conclusion

In summary, we have achieved the conversion of space-transmitted ultrafast lasers into optical fiber transmission by focusing the laser into a core of AR-HCF. This provides the potential for subsequent application simplicity in industrial settings. We compared the ultrafast laser transmission between air-filled and vacuum-pumped seven-capillary AR-HCF. The transmit efficiency and the pulse shape that are affected by the SPM were discussed, and the method of extracting air could provide a simple solution. Results showed an improvement in laser transmission efficiency in vacuum-pumped fiber, and the efficiency improved from 61% to 72% with the suppression of air concentration, and the pulse distortion phenomenon could also be suppressed. The pulse broadening from 500 fs to 670 fs was recorded and might be improved in the future by using a more powerful pump at a lower atmospheric pressure. In addition, by modifying the fiber's structure so that it could support SHG or THG lasers, the experimental results could serve as a guide for other flexible beam transmission projects.

Data availability statement

The raw data supporting the conclusions of this article will be made available by the authors, without undue reservation.

Author contributions

YC: Conceptualization, Methodology, Data Curation, Writing—Original Draft. YM: Visualization, Software, Formal analysis. SX: Data curation. JS: Investigation QZ: Investigation. RL: Resources. JL: Supervision, Project administration. CL: Supervision. DY: Supervision. YX: Supervision, Funding Acquisition, Resources, Supervision, Writing—Review and Editing.

Funding

This work was supported by National Natural Science Foundation of China (Nos. 61975061 and 61735007).

Conflict of interest

YM and RL were empolyed by Wuhan Raycus Fiber Laser Technologies Co., Ltd.

The remaining authors declare that the research was conducted in the absence of any commercial or financial relationships that could be construed as a potential conflict of interest.

Publisher's note

References

1. Phillips KC, Gandhi HH, Mazur E, Sundaram SK. Ultrafast laser processing of materials: A Review. *Adv Opt Photon* (2015) 7(4):684. doi:10.1364/aop.7.000684

2. Malinauskas M, Žukauskas A, Hasegawa S, Hayasaki Y, Mizeikis V, Buividas R, et al. Ultrafast laser processing of materials: From science to industry. *Light: Sci Appl* (2016) 5(8):e16133–e.

3. Sakakura M, Lei Y, Wang L, Yu Y-H, Kazansky PGJLS. Applications. Ultralow-loss geometric phase and polarization shaping by ultrafast laser writing in silica glass. *Light: Sci Appl* (2020) 9(1):1–10.

4. Han H, Wang R, Cao H, Wen X, Dai C, Liu W, et al. Coded information storage pulsed laser based on vector period-doubled pulsating solitons. *Opt Laser Tech* (2023) 158:108894. doi:10.1016/j.optlastec.2022.108894

5. Yu L, Wang B, Han H, Dai C, Liu W, Wang Y. Passively Q-switched operation based on Sb2se3 and self-power near infrared photodetector. *J Lumin* (2022) 244: 118704. doi:10.1016/j.jlumin.2021.118704

6. Smith AV, Do BT, Hadley GR, Farrow RL. Optical damage limits to pulse energy from fibers. *IEEE J Sel Top Quan Electron* (2009) 15(1):153–8. doi:10.1109/jstqe.2008.2010331

7. Cregan RF, Mangan BJ, Knight JC, Birks TA, Russell PSJ, Roberts PJ, et al. Single-mode photonic band gap guidance of light in air. *Science* (1999) 285(5433):1537–9. doi:10.1126/science.285.5433.1537

8. Ishaaya AA, Hensley CJ, Shim B, Schrauth S, Koch KW, Gaeta AL. Highly-efficient coupling of linearly- and radially-polarized femtosecond pulses in hollow-core photonic band-gap fibers. *Opt express* (2009) 17(21):18630–7. doi:10.1364/OE.17.018630

9. Knight JC. Photonic crystal fibres. *Nature* (2003) 424(6950):847–51. doi:10.1038/nature01940

10. Poletti F, Petrovich MN, Richardson DJ. Hollow-core photonic bandgap fibers: Technology and applications. *Nanophotonics* (2013) 2(5-6):315–40. doi:10.1515/nanoph-2013-0042

11. Gao SF, Wang YY, Liu XL, Hong C, Gu S, Wang P. Nodeless hollow-core fiber for the visible spectral range. *Opt Lett* (2017) 42(1):61–4. Epub 2017/01/07. doi:10.1364/OL.42.000061

12. Yu F, Cann M, Brunton A, Wadsworth W, Knight J. Single-mode solarization-free hollow-core fiber for ultraviolet pulse delivery. *Opt express* (2018) 26(8):10879–87. Epub 2018/05/03. doi:10.1364/OE.26.010879

13. Gao SF, Wang YY, Ding W, Wang P. Hollow-core negative-curvature fiber for uv guidance. *Opt Lett* (2018) 43(6):1347–50. Epub 2018/03/16. doi:10.1364/OL.43.001347

14. Pryamikov AD, Biriukov AS, Kosolapov AF, Plotnichenko VG, Semjonov SL, Dianov EM. Demonstration of a waveguide regime for a silica hollow - core microstructured optical fiber with a negative curvature of the core boundary in the spectral region > 3.5 μm. *Opt express* (2011) 19(2):1441–8. doi:10.1364/OE.19.001441

15. Yu F, Wadsworth WJ, Knight JC. Low loss silica hollow core fibers for 3–4 Mm spectral region. *Opt express* (2012) 20(10):11153–8. doi:10.1364/OE.20.011153

16. Yu F, Knight JC. Spectral attenuation limits of silica hollow core negative curvature fiber. *Opt express* (2013) 21(18):21466–71. Epub 2013/10/10. doi:10.1364/OE.21.021466

17. Chen Y, Wang Z, Gu B, Yu F, Lu Q. Achieving a 15 μm fiber gas Raman laser source with about 400 kW of peak power and a 63 GHz linewidth. *Opt Lett* (2016) 41(21):5118–21. Epub 2016/11/03. doi:10.1364/OL.41.005118

18. Kolyadin AN, Kosolapov AF, Pryamikov AD, Biriukov AS, Plotnichenko VG, Dianov EM. Light transmission in negative curvature hollow core fiber in extremely high material loss region. *Opt express* (2013) 21(8):9514–9. Epub 2013/04/24. doi:10.1364/OE.21.009514

19. Belardi W, Knight JC. Hollow antiresonant fibers with low bending loss. *Opt express* (2014) 22(8):10091–6. Epub 2014/05/03. doi:10.1364/OE.22.010091

20. Zhu X, Wu D, Wang Y, Yu F, Li Q, Qi Y, et al. Delivery of cw laser power up to 300 watts at 1080 Nm by an uncooled low-loss anti-resonant hollow-core fiber. *Opt express* (2021) 29(2):1492–501. Epub 2021/03/18. doi:10.1364/OE.415494

21. Cui Y, Huang W, Zhou Z, Li H, Wang M, Chen Z, et al. Highly efficient and stable coupling of kilowatt-level continuous wave laser into hollow-core fibers. *Chin Opt Lett* (2022) 20(4):040602. doi:10.3788/col202220.040602

22. Ouzounov DG, Ahmad FR, Müller D, Venkataraman N, Gallagher MT, Thomas MG, et al. Generation of megawatt optical solitons in hollow-core photonic band-gap fibers. *Science* (2003) 301(5640):1702–4. doi:10.1126/science.1088387

23. de Matos CJS, Taylor JR, Hansen TP, Hansen KP, Broeng J. All-fiber chirped pulse amplification using highly-dispersive air-core photonic bandgap fiber. *Opt express* (2003) 11(22):2832–7. doi:10.1364/OE.11.002832

24. Wu S, Siwicki B, Carter RM, Biancalana F, Shephard JD, Hand DP. Impact of nonlinear effects on transmission losses of hollow-core antiresonant negative curvature optical fiber. *Appl Opt* (2020) 59(16):4988–96. Epub 2020/06/17. doi:10.1364/AO.382350

25. Emaury, F, Saraceno, CJ, Dutin, CF, Wang, YY, Schriber, C, Gerome, F, et al. *Efficient femtosecond operation of a kagome-type hc-pcf fiber at 75 W average power. CLEO: Science and innovations*. San Jose, CA: Optica Publishing Group (2013).

26. Li F, Yang Z, Lv Z, Wang Y, Li Q, Wei Y, et al. High energy femtosecond laser micromachining with hollow core photonic crystal fiber delivery. *Optik* (2019) 194: 163093. doi:10.1016/j.ijleo.2019.163093

27. Machinet, G, Debort, B, Kling, R, Lopez, J, Gerome, F, Benabid, F, et al. *High average power and high energy transport of ultrashort pulses with a low loss kagome hollow-core photonic crystal fiber for micromachining. The European Conference on Lasers and electro-optics*. Munich, Germany: Optica Publishing Group (2013).

28. Kolyadin AN, Alagashev GK, Pryamikov AD, Mouradian L, Zeytunyan A, Toneyan H, et al. Negative curvature hollow-core fibers: Dispersion properties and femtosecond pulse delivery. *Phys Proced* (2015) 73:59–66. doi:10.1016/j.phpro.2015.09.122

29. Mousavi SA, Mulvad HCH, Wheeler NV, Horak P, Hayes J, Chen Y, et al. Nonlinear dynamic of picosecond pulse propagation in atmospheric air-filled hollow core fibers. *Opt express* (2018) 26(7):8866–82. Epub 2018/05/03. doi:10.1364/OE.26.008866

30. Debord B, Alharbi M, Vincetti L, Husakou A, Fourcade-Dutin C, Hoenninger C, et al. Multi-meter fiber-delivery and pulse self-compression of milli-joule femtosecond laser and fiber-aided laser-micromachining. *Opt express* (2014) 22(9):10735–46. Epub 2014/06/13. doi:10.1364/OE.22.010735

31. Gladyshev AV, Yatsenko YP, Kosolapov AF, Myasnikov DV, Bufetov IA. Propagation of megawatt subpicosecond light pulses with the minimum possible shape and spectrum distortion in an air- or argon-filled hollow-core revolver fibre. *Quan Elect* (2019) 49(12):1100–7. doi:10.1070/qel17156

32. Sung JH, Park JY, Imran T, Lee YS, Nam CH. Generation of 0.2-tw 5.5-fs optical pulses at 1 khz using a differentially pumped hollow-fiber chirped-mirror compressor. *Appl Phys B* (2005) 82(1):5–8. doi:10.1007/s00340-005-2005-0

33. Suda A, Hatayama M, Nagasaka K, Midorikawa K. Generation of sub-10-fs, 5-mj-optical pulses using a hollow fiber with a pressure gradient. *Appl Phys Lett* (2005) 86(11):111116. doi:10.1063/1.1883706

34. Sartania Zc S, Lenzner M, Tempea G, Spielmann C, Krausz F. Generation of 0.1-tw 5-fs optical pulses at a 1-khz repetition rate. *Opt Lett* (1997) 22:1562. doi:10.1364/ol.22.001562

35. Chakrabarti K, Mostufa S, Paul AK. Design and analysis of a position chirped metamaterial photonic crystal array for confinement of light pulses. *J Opt* (2021) 23(11): 115201. doi:10.1088/2040-8986/ac2164

36. Michieletto M, Lyngso JK, Jakobsen C, Laegsgaard J, Bang O, Alkeskjold TT. Hollow-core fibers for high power pulse delivery. *Opt express* (2016) 24(7):7103–19. Epub 2016/05/04. doi:10.1364/OE.24.007103

37. Marcatili EAJ, Schmeltzer RA. Hollow metallic and dielectric waveguides for long distance optical transmission and lasers. *Bell Syst Tech J* (1964) 43(4):1783–809. doi:10.1002/j.1538-7305.1964.tb04108.x

38. Winzer PJ, Leeb WR. Fiber coupling efficiency for random light and its applications to lidar. *Opt Lett* (1998) 23(13):986–8. doi:10.1364/OL.23.000986

39. Wei D, Ying-Ying W, Shou-Fei G, Yi-Feng H, Pu W. Theoretical and experimental investigation of light guidance in hollow-core anti-resonant fiber. *Acta Physica Sinica* (2018) 67(12):124201. doi:10.7498/aps.67.20180724

40. Li H, Goel C, Zang J, Raghuraman S, Chen S, Abu Hassan MR, et al. Integration of an anti-resonant hollow-core fiber with a multimode Yb-doped fiber for high power near-diffraction-limited laser operation. *Opt express* (2022) 30(5):7928. doi:10.1364/oe.451033

41. Goel C, Li H, Abu Hassan MR, Chang W, Yoo S. Anti-resonant hollow-core fiber fusion spliced to laser gain fiber for high-power beam delivery. *Opt Lett* (2021) 46(17): 4374–7. Epub 2021/09/02. doi:10.1364/OL.436054

42. Xiong D, Wu X, Abu Hassan MR, Gavara T, Chang W. In-line hollow-core fiber-optic bandpass filter. *Opt Lett* (2021) 46(23):5918–21. Epub 2021/12/02. doi:10.1364/OL.447108

43. Fibich G, Gaeta AL. Critical power for self-focusing in bulk media and in hollow waveguides. *Opt Lett* (2000) 25(5):335–7. doi:10.1364/OL.25.000335

44. Chraplyvy AR. Limitations on lightwave communications imposed by optical-fiber nonlinearities. *J Lightwave Tech* (1990) 8(10):1548–57. doi:10.1109/50.59195